

# Measurement and prediction of nonlinearity in outdoor propagation of periodic signals<sup>a)</sup>

Kent L. Gee<sup>b)</sup> and Victor W. Sparrow

Graduate Program in Acoustics, 202 Applied Science Bldg., The Pennsylvania State University, University Park, Pennsylvania 16802

Michael M. James,<sup>c)</sup> J. Micah Downing,<sup>c)</sup> and Christopher M. Hobbs

Wyle Laboratories, 2001 Jefferson Davis Hwy. Ste. 701, Arlington, Virginia 22202

(Received 10 October 2005; revised 3 August 2006; accepted 5 August 2006)

Far field propagation measurements of high-amplitude periodic signals generated by the U. S. Army Research Laboratory's Mobile Acoustic Source (MOAS) have been made. The MOAS is a large horn-coupled electropneumatic loudspeaker capable of producing sound at a few hundred hertz with a maximum overall sound pressure level of 155 dB *re* 20  $\mu$ Pa at 1 m. The possible influence of nonlinear effects have been investigated because the measurements exhibit greater sound pressure levels at high harmonics than are predicted by a linear propagation model. Between 100 and 375 m, nonlinearly predicted spectra obtained via a generalized Burgers equation-based model are consistently closer to measured spectra than are linear predictions, according to calculations of mean absolute error. These comparisons strengthen the assertion that nonlinearity is, in fact, the primary cause of disagreement between the measured and linearly predicted spectra at high frequencies. Comparisons between the nonlinear model and measurements, however, yield increased errors for greater propagation distances ( $\sim$ 1 km) and for measurements made later in the afternoon. For these cases, the nonlinear model calculations generally predict greater sound pressure levels at high frequencies than are actually present in the MOAS measurements. Despite the increased errors for these latter comparisons, the nonlinear model still typically performs better than the linear model. This provides additional confirmation of the presence of nonlinearity in the propagation, but may also point to the need to account for atmospheric variability in the numerical model to provide improved predictions. © 2006 Acoustical Society of America. [DOI: 10.1121/1.2345934]

PACS number(s): 43.25.Cb [MFH]

Pages: 2491–2499

## I. INTRODUCTION

In the past, the role of nonlinearity in the propagation of high-amplitude sound has been given considerable attention in a variety of contexts. Relevant studies have utilized analytical, numerical, and experimental methods to study various aspects of the problem. However, a review of the literature reveals only a limited number of experiments dedicated to the measurement of finite-amplitude effects in outdoor continuous-wave sound propagation. Theobald<sup>1</sup> studied the vertical propagation of periodic waveforms over a maximum range of 76 m. Webster and Blackstock<sup>2</sup> subsequently performed a similar study over a comparable range with band-limited noise waveforms. Both of these studies showed clear evidence of nonlinear propagation in that the measured high-frequency sound pressure levels were significantly greater than those predicted with linear theory.

Our main purpose in this article is to describe the results of recent field experiments with a high-amplitude acoustic

source that also show evidence of nonlinear effects. The source for these measurements was the U. S. Army Research Laboratory's Mobile Acoustic Source<sup>3</sup> (MOAS), which is a large electropneumatic loudspeaker. These experiments with the MOAS have been carried out as part of a multifaceted effort to study nonlinearity in the propagation of noise from high-performance jet aircraft<sup>4</sup> over moderate ranges. Because of the potential impact that takeoffs and low-altitude training runs may have on nearby communities, nonlinearity in ground-to-ground propagation is of considerable interest. Consequently, these controlled-source measurements were conducted over several hundred meters at near-grazing incidence, for which ground effects can play a considerable role. Also, as is typical with outdoor propagation experiments, wind, turbulence, and temperature profiles affect the recorded waveforms.

Because multiple phenomena influence the propagation, an important aspect of the measurement analysis is a comparison against the results of a numerical model<sup>5</sup> that is based on the generalized Burgers equation (GBE). The GBE is a widely established nonlinear model equation that can correctly predict the effects of second-order nonlinearity for lossy parabolic propagation of acoustic pressure waveforms. However, because the GBE does not incorporate all the phenomena that affect outdoor measurements, a comparison of

<sup>a)</sup>Portions of this research were presented at the 148th meeting of the Acoustical Society of America in San Diego, California, November 2004.

<sup>b)</sup>Current address: Department of Physics and Astronomy, N319 ESC, Brigham Young University, Provo, Utah 84602; electronic mail: kentgee@byu.edu

<sup>c)</sup>Current address: Blue Ridge Research and Consulting, LLC., 13 1/2 W. Walnut St., Asheville, North Carolina 28801.



FIG. 1. (Color online) Photograph of the U.S. Army Research Laboratory's Mobile Acoustic Source (MOAS).

the numerical results against the measurement may give some indication of the relative importance of nonlinear effects at a given frequency for a particular test. Theobald<sup>1</sup> also made numerical comparisons against his periodic-waveform measurements using a modified form of an algorithm developed by Pestorius and Blackstock.<sup>6</sup> Agreement between measured versus numerically calculated levels for the first three harmonics was good over short distances, but significantly worsened for the second and third harmonics by the maximum measurement distance of 76 m. Computed results were obtained using only one cycle of the input waveform that was scaled to match the time-averaged level of the fundamental frequency.

In the remainder of this paper, the MOAS and the measurement setup are first described. Measurement results for a number of cases are then presented and discussed. Finally, after a brief discussion of the numerical model, comparisons between measured and both nonlinearly and linearly predicted spectra are examined and analyzed.

## II. MEASUREMENT SUMMARY

### A. The mobile acoustic source

The U. S. Army Research Laboratory has a large horn-coupled electropneumatic loudspeaker known as the Mobile Acoustic Source (MOAS). The horn is a 10-Hz exponential horn that is 17.1 m long and has a mouth diameter of 2.3 m. Acoustic pressure signals are generated by a valve that modulates the flow of compressed air. The MOAS, which has a nominal frequency response range of 10–500 Hz, was primarily designed to simulate the acoustical signature of a tank. Measurements of the MOAS conducted by the National Center for Physical Acoustics at the University of Mississippi<sup>7</sup> indicate maximum output levels of 155 dB *re* 20  $\mu$ Pa at 1 m. The MOAS is shown mounted on its flatbed trailer in Fig. 1, where the horn's axis is located 3 m above the ground.

### B. Measurement array and environment

The propagation measurements were conducted on 12 February 2004 at the Blossom Point field test facility in Blossom Point, MD between 13:00 and 14:45 Eastern Standard Time (EST). Bruel and Kjaer 12.7-mm free-field microphones (Type 4190) were located along the loudspeaker centerline according to the layout in Fig. 2. Microphone poles were placed at 10, 100, 250, and 375 m, and an existing tower was used to collect data at 1092 m. The measurement elevation angles were 0°, 0.7°, and 1.4°, relative to the 10-

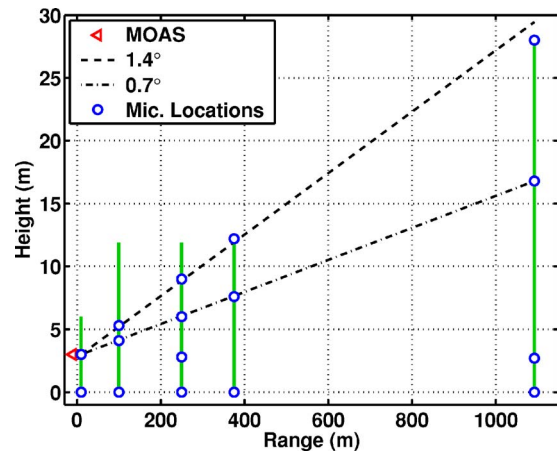


FIG. 2. (Color online) Microphone ranges and heights for the MOAS propagation measurements.

m on-axis microphone. The 1.4° measurement angle is approximate because the tower height was insufficient to place the 1092-m microphone along the same angle as the rest of the microphones, which were located nominally at 1.45°. Microphones were also placed on the ground at each pole location and at the tower. All microphones were pointed at the source (normal incidence), which yields a nominally flat ( $\pm 1$  dB) amplitude response for the Type 4190 microphones out to 20 kHz. With the exception of the tower data at 1092 m, microphone data acquisition was carried out using National Instruments 24-bit PXI-4472 cards sampling at 96 kHz. At the tower, waveform data were acquired with a National Instruments 16-bit NI-DAQ 6036-E card sampling at 200 kHz and were then multiplexed over four channels, yielding an effective sampling frequency of 50 kHz per channel.

The ground along the propagation path was fairly flat, nominally soft, and covered by long grass and other vegetation. Because of hardware failure, meteorological information at the site was not recorded during the measurements. However, data from the Naval Surface Warfare Center Dahlgren laboratory located approximately 10 km (6 mi) from the measurement site provided a reasonable estimate of average weather conditions based on a comparison between Blossom Point and Dahlgren data made the day before.

According to the Dahlgren data, between 13:00 and 14:45 EST, the ambient pressure was approximately constant at 1.0 atm, the temperature range was 4 °–5 °C, and the relative humidity varied between 70% and 77%. Wind speeds ranged between 1 and 6 m/s with a variable direction. Because of the uncertainty in the ambient conditions, the values for atmospheric absorption and dispersion calculations in the propagation model were assumed to be constant at 1 atm for ambient pressure, 4 °C for temperature, and 73% for relative humidity.

### C. Measured waveforms

For the propagation measurements, a variety of periodic waveforms with fundamental frequencies ranging from 50–400 Hz were used as signal inputs. Sine, triangle, and square waves were all used, but the MOAS frequency re-

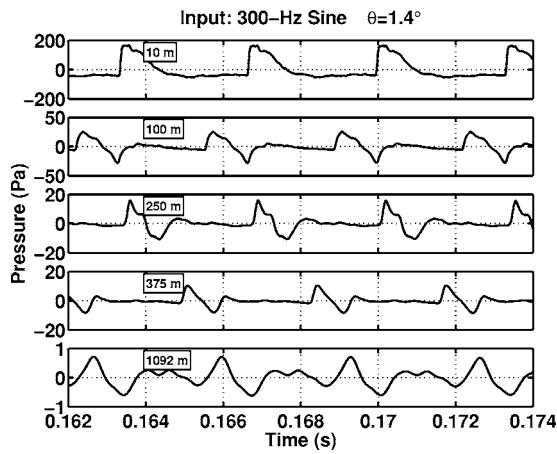


FIG. 3. Measured MOAS waveforms along  $1.4^\circ$  for a 300-Hz input sine wave. Distance labels correspond to the microphone ranges shown in Fig. 2.

sponse and inherent distortion were such that its ability to acoustically transmit the supplied electrical signals was rather poor. Consequently, the type of input waveform was later found to be largely irrelevant. In addition to the periodic signals described, pink noise was also used. However, the limited frequency response of the MOAS resulted in a natural bandpass filtering of the noise signal and, consequently, significantly lower amplitudes for the pink noise tests.

As an example of a typical measurement, recorded waveforms along  $1.4^\circ$  for a 300-Hz sine wave input are shown in Fig. 3. Although a sinusoidal electrical signal was supplied, the resultant waveform at 10 m is quite nonsinusoidal and significantly skewed, but it is periodic with a fundamental frequency of 300 Hz. The waveform skewness at close range could be related to the compressed-air nature of the source that results in a net volume increase over a cycle. Similarly skewed, nonsinusoidal waveforms recorded at close range for a 100-Hz sinusoidal input to the MOAS have been reported by Sabatier.<sup>7</sup>

#### D. Measured spectra as a function of range

Because the difference between nonlinear and linear propagation is often greatest at high frequencies that are not readily visible in time waveform comparisons, the emphasis hereafter will be on trends in the measured and predicted spectra at these frequencies. The measured spectra for the 300-Hz test waveforms shown previously in Fig. 3 along  $1.4^\circ$  are displayed in Fig. 4. For purposes of clarity, only the levels at each of the harmonic frequencies, rather than full spectra, are displayed. The overall sound pressure level (OASPL) for each spectrum is located in the figure legend. Approximately 11 s of data were used to calculate the PSD for each case, both to allow fine-scale spectral resolution and to mitigate the effect of fluctuations in waveform amplitudes caused by wind variability. The measured harmonic levels for the same 300-Hz sine wave test, but along  $0.7^\circ$ , are shown in Fig. 5. Similar spectral results are obtained for both propagation angles at most distances, but there are some notable differences in the rates of high-frequency spectral decay of the 1092-m spectra. This greater variability, which is

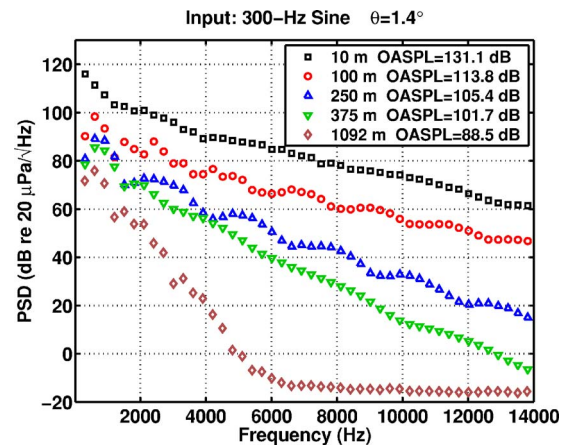


FIG. 4. (Color online) Measured MOAS harmonic levels along  $1.4^\circ$  for a 300-Hz input sine wave. In this as well as subsequent figures, OASPL signifies overall sound pressure level and is referenced to  $20 \mu\text{Pa}$ .

seen in the majority of the 1092-m measurements, directly impacts the ability to model the propagation out to that distance.

Some discussion of observed ground effects in the spectra is also merited. The broadband spectral results of a propagation measurement with a pink noise input are helpful in this regard. Displayed in Fig. 6 are measured spectra for a pink noise along  $0.7^\circ$ . A comparison of these spectra with those from the 300-Hz sine wave test in Fig. 5 reveal the presence of several spectral minima that occur at similar frequencies. In Fig. 6, the lowest frequencies at which a spectral minimum occurs for each curve (e.g., approximately 85 Hz at 10 m and 250 Hz at 100 m) closely matches those predicted by a ground reflection model using flow resistivity values corresponding to soft terrain. The particular ground interaction model used accounts for the interaction of spherically spreading waves with a finite-impedance ground<sup>8</sup> as well as the effects of atmospheric turbulence.<sup>9</sup> The results of the ground reflection model and the consistency of the measured frequencies of the lowest spectral minima indicate that these minima are due to the superposition of the direct and ground-reflected waveforms at the microphone. At higher frequencies, spectral minima are not nearly as defined. This

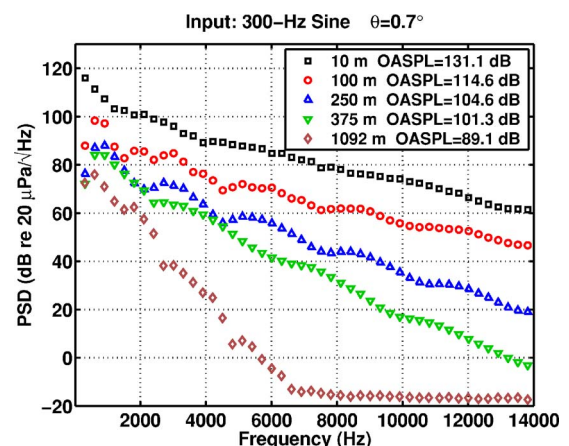


FIG. 5. (Color online) Measured MOAS harmonic levels along  $0.7^\circ$  for a 300-Hz input sine wave.

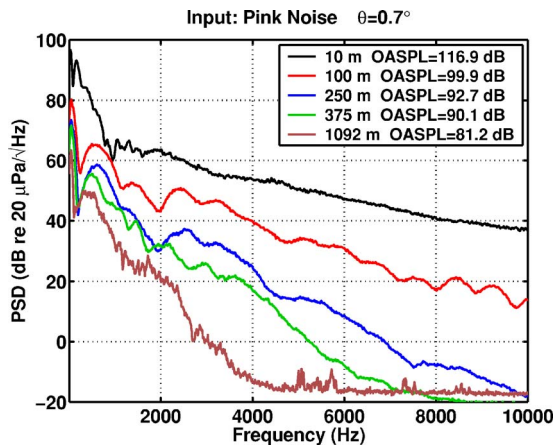


FIG. 6. (Color online) Measured MOAS spectra along  $0.7^\circ$  for input pink noise.

minima broadening is likely caused by atmospheric turbulence and is predicted by the ground reflection model when turbulence is included. Because the frequencies at which these minima occur also vary somewhat from test to test, other atmospheric inhomogeneities and curved ray propagation likely influence some of the measurements.

Spectral calculations as a function of range have been made for many more cases; however, the spectra shown are sufficient to highlight important aspects of the measurements obtained, as well as to point out the measurement system noise floor. Consideration of the system noise floor is particularly important in analyses of the 375-m and 1092-m data. From the preceding figures, it is evident that for the microphones mounted on the pole at 375 m, the system noise floor was approximately  $-20$  dB re  $20 \mu\text{Pa}/\sqrt{\text{Hz}}$ . For the 1092-m data, the noise floor was about  $-15$  dB re  $20 \mu\text{Pa}/\sqrt{\text{Hz}}$ . Given these noise floors, the upper frequency limit of all analyses presented hereafter has been limited to where the signal-to-noise ratio is approximately 10 dB.

### E. Measured spectra as a function of height

One other important aspect in describing the measurement is to consider the stability and quiescence of the atmosphere, because atmospheric homogeneity is assumed in the numerical model. Unfortunately, because detailed meteorological data at the measurement site are not available, an alternate means of examining the local atmospheric conditions has been used. The effect of the atmosphere on acoustic propagation may be studied by comparing spectra as a function of microphone height at the same range. For a perfectly still, homogeneous atmosphere, there should be general agreement between harmonic levels for the  $0.7^\circ$  and in  $1.4^\circ$  microphones at a given range. There will be differences in individual harmonics, caused by the differences in the direct and ground-reflected paths as a function of height, but the overall trend in spectral decay as a function of frequency should remain the same. Variation from a common trend for different microphone heights indicates some form of atmospheric variability.

Harmonic levels at 375 m are shown as a function of height for two cases: the 300-Hz sine wave test previously

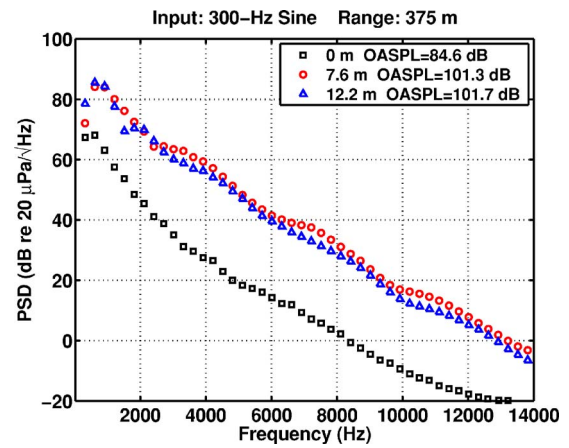


FIG. 7. (Color online) Measured MOAS harmonic levels at three microphone heights at a range of 375 m for a 300-Hz input sine wave. The time of the test was 13:34 EST.

discussed, which occurred at 13:34 EST, and a 400-Hz square wave test conducted at 14:33 EST. The results for these two tests typify the change in ambient conditions that occurred during the latter measurements. Displayed in Figs. 7 and 8 are harmonic spectral levels as a function of microphone height at 375 m for the 300-Hz sine wave and 400-Hz square wave tests, respectively. As may be anticipated, the microphones located on the ground in both cases yield lower levels than for those microphones located off the ground. This is likely due to the additional losses caused by propagation along the ground at grazing incidence; consequently, ground microphone data are not considered further. For the microphones located off the ground, however, there is a significantly different behavior between the two tests with regard to the harmonic amplitudes at 7.6 m ( $0.7^\circ$ ) and 12.2 m ( $1.4^\circ$ ). For the 300-Hz test, the  $0.7^\circ$  levels are only slightly greater than the  $1.4^\circ$  levels at high frequencies. However, for the 400-Hz square wave test, the differences are much greater and increase as a function of frequency. This comparison implies that an assumption of a quiescent, homogeneous atmosphere is less appropriate for measurements taken toward the end of the day. This apparent degra-

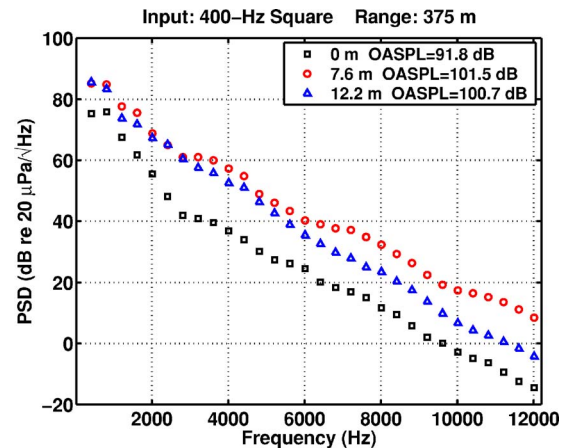


FIG. 8. (Color online) Measured MOAS harmonic levels at three microphone heights at a range of 375 m for a 400-Hz input square wave test made later in the afternoon, at 14:33 EST.

dation of stable atmospheric conditions for later tests directly impacts accompanying propagation predictions made using the numerical model described below.

Although this summary of the complete MOAS field experiment has been carried out with relatively few cases, the waveforms and spectra shown are representative of the entire test. After a brief overview of the numerical model used to obtain nonlinear and linear propagation predictions, comparisons between measured and predicted spectra for various cases are presented and discussed.

### III. NUMERICAL MODEL OVERVIEW

#### A. The generalized Burgers equation

In this section, the nonlinear numerical model used in the comparisons against the MOAS field experiment is described. A parabolic model equation that has been used extensively to treat the problem of nonlinear propagation through a lossy medium is the Burgers equation. In its most basic form, the Burgers equation describes plane-wave propagation through a thermoviscous medium; however, other formulations have incorporated geometrical spreading<sup>10</sup> and arbitrary absorption and dispersion.<sup>11</sup> One form of the generalized Burgers equation (GBE), on which the numerical model is based, may be written for assumed spherical spreading as

$$\frac{\partial p}{\partial r} = \frac{\beta}{2\rho_0 c_0^3} \frac{\partial p^2}{\partial \tau} + \psi(\tau)p - \frac{1}{r}p. \quad (1)$$

In Eq. (1),  $p(r, \tau)$  is the acoustic pressure,  $r$ , the range variable,  $\beta$ , the coefficient of nonlinearity,  $\rho_0$ , the ambient density,  $c_0$ , the small-signal sound speed,  $\tau = t - (r - r_0)/c_0$ , the retarded time of propagation between  $r_0$  and  $r$ , and  $\psi(\tau)$ , a generalized absorption and dispersion operator that acts on  $p$ . In the context of the current propagation problem,  $\psi(\tau)$  represents atmospheric absorption and dispersion. An additional term may be included in the GBE to treat atmospheric stratification (e.g., see Ref. 12), but because atmospheric inhomogeneity is not modeled in this work, the term has been neglected.

#### B. GBE solution technique

The solution technique to the GBE employed in this research is an adaptation from previous work carried out at the University of Texas at Austin and the University of Mississippi, where hybrid time-frequency domain nonlinear propagation algorithms have been developed and refined. The time-frequency domain solution method originated with Pestorius and Blackstock,<sup>6</sup> who investigated finite-amplitude noise propagation in a one-dimensional tube and developed an algorithm to numerically propagate acoustic pressure waveforms. The nonlinear portion of the propagation was carried out in the time domain, and the small-signal portion of the propagation (boundary-layer absorption and dispersion) was handled in the frequency domain. Pierce<sup>13</sup> has demonstrated that the ‘‘Pestorius algorithm’’ reduces to the GBE appropriate for plane-wave propagation in a one-dimensional duct.

Anderson<sup>14</sup> developed an alternative to the Pestorius algorithm in his study of spherically decaying  $N$  waves. To eliminate the need for weak shock theory, which Pestorius’ method employed, adaptive step sizing was used to ensure that the waveform was singly valued for all range steps. Following Anderson’s initial work, improvements to the ‘‘Anderson algorithm’’ were made by others also interested in the nonlinear propagation of transients.<sup>15–17</sup>

The present numerical solution to the GBE in Eq. (1) has been developed from a study of the Pestorius and Anderson methodologies. The algorithm most closely resembles the Anderson approach because it employs an adaptive step size. However, because Anderson’s code and its subsequent modifications have been intended primarily for the propagation of transients, some elements of the model are more closely linked to the work of Pestorius, who dealt with continuous-wave signals. Implementation details for the model may be found in Ref. 5.

### IV. COMPARISON RESULTS AND ANALYSIS

In this section, comparisons are made between measured spectra and predicted spectra obtained by numerically propagating recorded waveforms both linearly and nonlinearly. The linear predictions, which have been obtained by removing the nonlinear term from Eq. (1), are equivalent to free-field extrapolations of the input spectrum using atmospheric absorption and spherical spreading. Use of approximately 11 s of data (2<sup>20</sup> samples) in the numerical propagation constitutes a significant difference from Theobald’s study, in which only a single cycle of the recorded waveform was used.<sup>1</sup> As with the PSD calculations in Sec. II, the use of relatively long waveforms as inputs to the numerical models allows for both fine-scale resolution and a large number of ensemble averages when calculating a predicted PSD. Note that a long input waveform and a greater number of averages are not expected to reduce errors between measured and predicted spectra if atmospheric and ground effects cause the actual propagation path to significantly differ from the straight numerical propagation path. An increased waveform length, however, has been found to help minimize variability in predicted spectra caused by wind-induced waveform amplitude fluctuations. Finally, data collected at 100 m, rather than at 10 m, have been used as inputs to the model because the 10-m on-axis microphone was found to be located within the geometrical near field of the MOAS, where an assumption of spherical spreading is not valid.<sup>5</sup>

In order to quantitatively compare the results of the nonlinear and linear models, an assessment of the overall error of a given model relative to the measurement is needed. The metric that has been selected for the purpose of these comparisons is the mean absolute error, in dB, between the measured PSD and a predicted PSD. For example, the mean absolute error,  $\overline{E_{M,N}}$ , between the measured PSD ( $\text{PSD}_M$ ) and nonlinearly predicted PSD ( $\text{PSD}_N$ ) may be written as

$$\overline{E_{M,N}} = \langle |\text{PSD}_M - \text{PSD}_N| \rangle, \quad (2)$$

where  $\langle \rangle$  is the expectation operator and the spectral densities are calculated in dB. The mean absolute error between

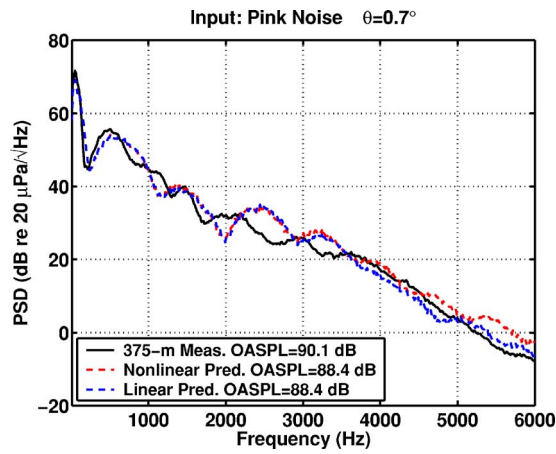


FIG. 9. (Color online) Measured and predicted spectra at 375 m,  $\theta=0.7^\circ$ , for pink noise input. The input for the predictions was the measured waveform at 100 m.

the measurement and linear prediction,  $\overline{E_{M,L}}$ , is calculated by replacing  $\text{PSD}_N$  in Eq. (2) with the linearly predicted PSD ( $\text{PSD}_L$ ). In each of the comparisons between measurement and model,  $\overline{E_{M,N}}$  and  $\overline{E_{M,L}}$  are calculated over the frequency range where the measured levels are at least 10 dB above the system noise floor.

The comparisons that follow are broken into two broad categories. First, results from the pink noise test are analyzed because its relatively low OASPL at 100 m make the test suitable as a sort of linear benchmark between the real-world data and the simplified models. Next, comparisons between the results from various tests with periodic waveforms are made and analyzed.

### A. Pink noise comparison

The OASPL of the pink noise spectrum at 100 m was 99.9 dB *re* 20  $\mu\text{Pa}$  (see Fig. 6), which is significantly lower than the tests with periodic waveforms. This case is useful in determining the level of agreement between the models and the measurement that is achieved when nonlinear effects appear to be minimal and when the atmosphere is relatively homogeneous. For this comparison, the recorded 100-m waveform at  $0.7^\circ$  has been propagated out to 375 m.

Shown in Fig. 9 is the measured 375-m PSD for  $0.7^\circ$ , along with the nonlinearly and linearly predicted spectra calculated from numerical propagation from 100 m. The nonlinear and linear predictions differ noticeably above 3.5 kHz, but result in the same predicted OASPL (88.4 dB *re* 20  $\mu\text{Pa}$ ) and generally follow the decay of the measured PSD out to 6 kHz. For this case,  $\overline{E_{M,N}}$  and  $\overline{E_{M,L}}$  are, respectively, 2.9 and 2.6 dB, which means that the linear prediction has slightly less error than the nonlinear prediction but both models have less than 3 dB of mean absolute error between 0 and 6 kHz. The maximum difference between both models and the measurement occurs at about 2.5 kHz, where a relative spectral maximum at 100 m is propagated outward with a free-field assumption and is then compared to a measured relative spectral minimum at 375 m. This maximum error is likely due to differences in multipath interference effects at higher frequencies. This pink noise comparison indicates that the

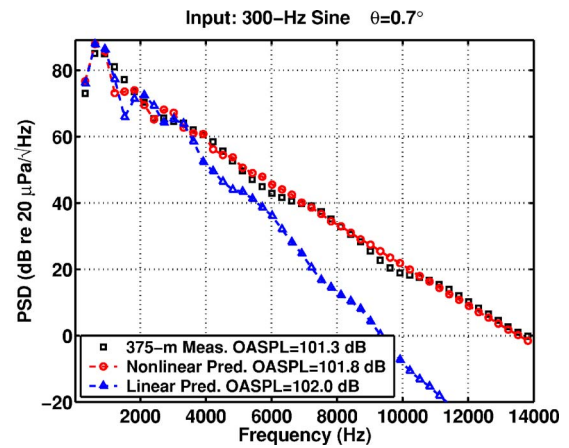


FIG. 10. (Color online) Measured and predicted harmonic levels at 375 m,  $\theta=0.7^\circ$  for a 300-Hz input sine wave. The input for the predictions was the measured waveform at 100 m.

linear and nonlinear free-field models are useful for comparing with general trends observed in the measured spectra when the atmosphere is reasonably homogeneous. It also indicates, however, that agreement at specific frequencies may be poor because of the variation in multipath interference as a function of range.

## B. Periodic signal comparisons

### 1. 100–375-m comparisons

The first set of comparisons with periodic source waveforms is carried out between 100 and 375 m, as was done with the pink noise test. The fact that virtually all periodic waveform measurements made over this range reveal a significant difference between linearly predicted and measured spectra at high frequencies suggests that nonlinearity influences the propagation. The results of comparisons between the measurement and the numerical predictions for three cases are now shown: the previously discussed 300-Hz sine-wave test along both  $0.7^\circ$  and  $1.4^\circ$  (see Figs. 4 and 5), as well as a 400-Hz sine-wave test along  $0.7^\circ$ . The 300-Hz measurement and predictions at 375 m along  $0.7^\circ$  and  $1.4^\circ$  are, respectively, shown in Figs. 10 and 11. The 400-Hz results along  $0.7^\circ$  are displayed in Fig. 12. Again, only the levels at each of the harmonics are shown for purposes of clarity. Calculations of  $\overline{E_{M,L}}$  and  $\overline{E_{M,N}}$  are shown in Table I for each of the three tests. Both the graphical and tabulated results reveal that the nonlinearly predicted spectra match the measurements significantly better than the linear predictions. As with the pink noise comparison, there are significant discrepancies at individual frequencies, but  $\overline{E_{M,N}} < 3$  dB for each of these cases. These comparisons indicate that nonlinear propagation is the primary cause of the discrepancy between linearly predicted and measured spectral levels at high frequencies.

### 2. 100–1092-m comparisons

The results for the 100-375-m comparisons confirm that nonlinear effects are present in the propagation of periodic signals from the MOAS. Another point of discussion is the influence of nonlinearity in the propagation beyond 375 m

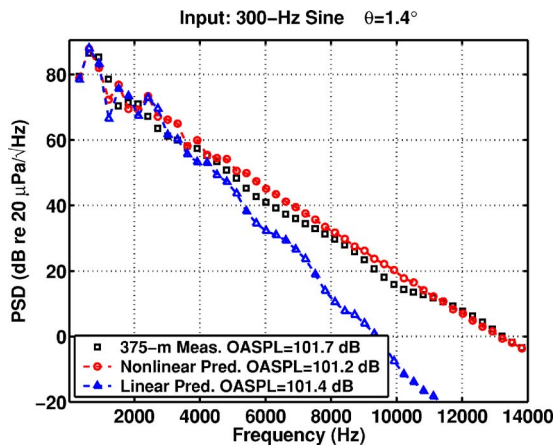


FIG. 11. (Color online) Measured and predicted harmonic levels at 375 m,  $\theta=1.4^\circ$  for a 300-Hz input sine wave. The input for the predictions was the measured waveform at 100 m.

out to 1092 m. The 300-Hz sine-wave test discussed previously was selected for study because of the good agreement achieved between the nonlinear model and measurement between 100 and 375 m. The 100-m waveforms at  $0.7^\circ$  and  $1.4^\circ$  were again used as inputs and this time were propagated out to 1092 m using the nonlinear and linear models. The results of the spectral comparisons are displayed in Figs. 13 and 14 and the mean absolute errors calculated in Table II. Although these results are not shown, nearly identical graphical and quantitative results were obtained when the 375-m recorded waveforms, rather than the 100-m recorded waveforms, were used as inputs to the model. In both cases considered here, as well as for the majority of other measurements performed, the nonlinearly predicted harmonic levels at 1092 m are consistently greater than the measured levels and yield a greater mean absolute error than the 100–375-m comparisons. For the  $0.7^\circ$  propagation angle,  $\overline{E_{M,L}}$  is still significantly greater than  $\overline{E_{M,N}}$ , but for  $1.4^\circ$ , the two error calculations are approximately equal.

The trends seen in the  $1.4^\circ$  results for the 300-Hz test are common for several different tests at one or sometimes both propagation angles in that  $\overline{E_{M,L}}$  and  $\overline{E_{M,N}}$  are nearly

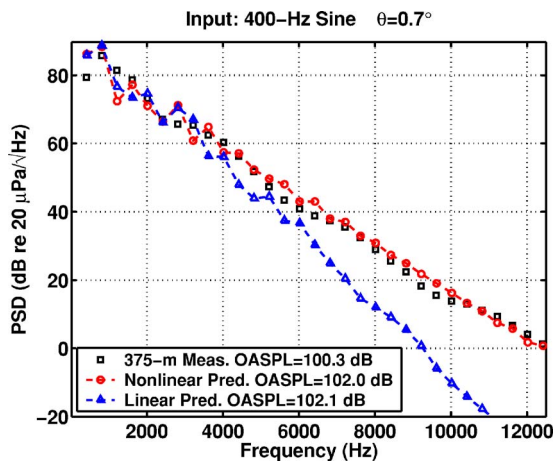


FIG. 12. (Color online) Measured and predicted harmonic levels at 375 m,  $\theta=0.7^\circ$  for a 400-Hz input sine wave. The input for the predictions was the measured waveform at 100 m.

TABLE I. Linear and nonlinear mean absolute errors, in dB, for the 100–375-m comparisons in Figs. 10–12. See Eq. (2) and the accompanying text for the definitions of  $\overline{E_{M,L}}$  and  $\overline{E_{M,N}}$ .

Frequency/angle	$\overline{E_{M,L}}$	$\overline{E_{M,N}}$
300-Hz/ $0.7^\circ$	17.9	1.6
300-Hz/ $1.4^\circ$	16.2	2.6
400-Hz/ $0.7^\circ$	13.6	2.5

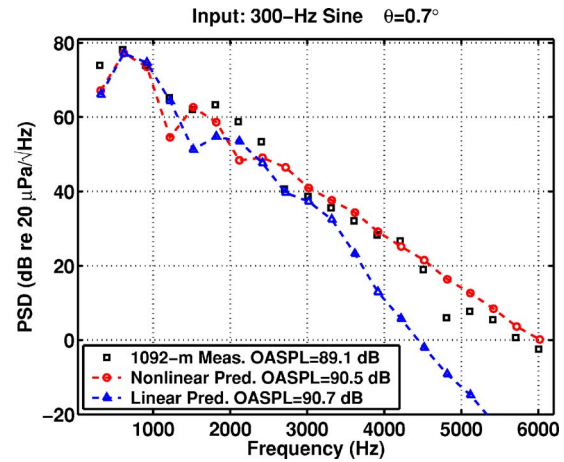


FIG. 13. (Color online) Measured and predicted harmonic levels at 1092 m,  $\theta=0.7^\circ$  for a 300-Hz input sine wave. The input for the predictions was the measured waveform at 100 m.

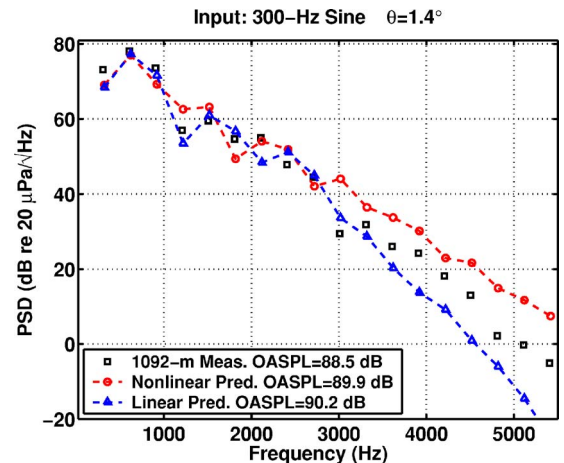


FIG. 14. (Color online) Measured and predicted harmonic levels at 375 m,  $\theta=1.4^\circ$  for a 300-Hz input sine wave. The input for the predictions was the measured waveform at 100 m.

TABLE II. Linear and nonlinear mean absolute errors, in dB, for the 100–1092-m comparisons in Figs. 13 and 14. See Eq. (2) and accompanying text for the definitions of  $\overline{E_{M,L}}$  and  $\overline{E_{M,N}}$ .

Frequency/angle	$\overline{E_{M,L}}$	$\overline{E_{M,N}}$
300-Hz/ $0.7^\circ$	12.2	3.9
300-Hz/ $1.4^\circ$	6.2	6.4

equal and the measured spectrum falls between the nonlinear and linear predictions. Although the exact cause of the general increased disagreement between nonlinearly predicted and measured spectra over the larger propagation range has not been ascertained, some qualitative discussion is merited. Generally good agreement between the 300-Hz measurement and the nonlinear model was achieved for the 100–375-m comparisons, despite neglecting phenomena such as ground effects, turbulence, and a nonuniform atmosphere. Over a significantly longer range, each phenomenon could more significantly affect the rate of nonlinear energy transfer in the propagating waveform. As an example, the effects of turbulence, while often negligible over shorter distances, would certainly play a larger role over an increased propagation range. The results of a study of the average effect of turbulence on shock-wave rise times<sup>18</sup> have indicated that a steepened waveform passing through turbulence unsteepens more quickly than for passage through a quiescent medium. A more rapid unsteepening could account for the experimentally observed accelerated reduction in the high-frequency sound pressure levels. Also, a homogeneous, quiescent atmosphere and straight-ray propagation have been assumed in the numerical calculations, whereas the influence of a realistic sound-speed profile and curved rays could substantially affect the measured results at a given microphone over a longer range. For example, upwind propagation could cause ray tube divergence, thereby reducing sound amplitudes along a given ray and slowing the rate of nonlinear distortion.

### 3. Comparisons for later measurements

Another comparison that shows the potential for meteorological affects to influence the ability to measure nonlinearity may be made with the 400-Hz square wave measurement made later in the afternoon. It was shown previously in the discussion of measured spectra as a function of microphone height that this measurement exhibited increased dependence of level on height at high frequencies relative to earlier tests (cf. Figs. 7 and 8). In conjunction with this apparent decrease in atmospheric homogeneity, concordance between nonlinear model and measurement significantly

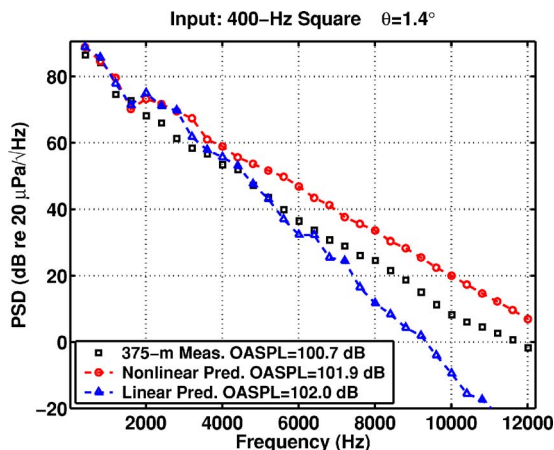


FIG. 15. (Color online) Measured and predicted harmonic levels at 375 m,  $\theta=1.4^\circ$  for a 400-Hz input square wave. The input for the predictions was the measured waveform at 100 m.

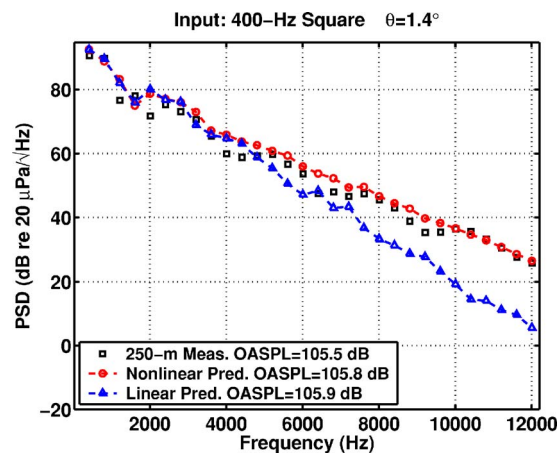


FIG. 16. (Color online) Measured and predicted harmonic levels at 250 m,  $\theta=1.4^\circ$  for a 400-Hz input square wave. The input for the predictions was the measured waveform at 100 m.

lessens. Figure 15 compares the  $1.4^\circ$  measured harmonic levels at 375 m with those predicted from numerical propagation from 100 m for the 400-Hz square wave test. The 100-m-based numerical calculation significantly overpredicts the measured sound pressure levels at high frequencies. To further investigate the cause of this discrepancy, the numerical propagation path was divided up using the intermediate measurement at 250 m (cf. Fig. 2) and separate calculations were performed for the 100–250-m and 250–375-m ranges. The results of these comparisons are shown in Figs. 16 and 17, respectively. Although the algorithm continues to slightly overpredict the spectral levels between 250 and 375 m, agreement is substantially better over the shorter propagation distances. The agreement is quantified with calculations of  $E_{M,L}$  and  $E_{M,N}$  in Table III. The fact that significantly better agreement is achieved with these shorter-range calculations than with the full 100–375-m range indicates that atmospheric effects can greatly impact conclusions regarding the nonlinearity of the propagation, even over relatively short distances.

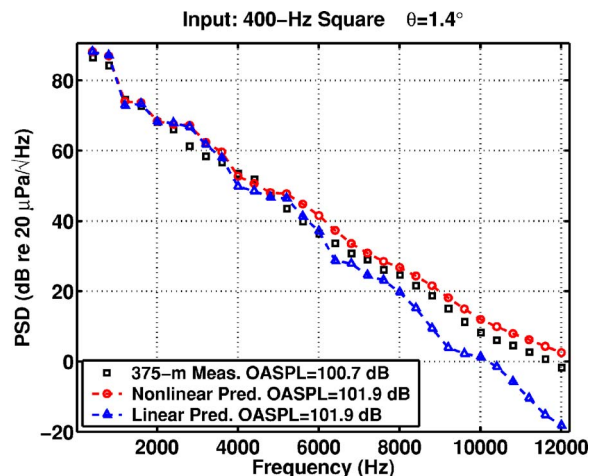


FIG. 17. (Color online) Measured and predicted harmonic levels at 375 m,  $\theta=1.4^\circ$  for a 400-Hz input square wave. The input for the predictions was the measured waveform at 250 m.

TABLE III. Linear and nonlinear mean absolute errors, in dB, for the 400-Hz square-wave test comparisons in Figs. 15–17. See Eq. (2) and the accompanying text for the definitions of  $\overline{E_{M,L}}$  and  $\overline{E_{M,N}}$ .

Range	$\overline{E_{M,L}}$	$\overline{E_{M,N}}$
100–375 m	9.1	7.8
100–250 m	8.0	2.7
250–375 m	5.3	2.9

## V. CONCLUSIONS

Finite-amplitude propagation effects have been measured in the outdoor propagation of periodic signals generated using the U.S. Army Research Laboratory’s Mobile Acoustic Source (MOAS). For most cases, the results of the nonlinear model based on the generalized Burgers equation compare favorably with the measurement and demonstrate significantly less mean absolute error than results from a linear model. This is true despite the fact that the nonlinear model assumes free-field propagation through a homogenous atmosphere and therefore neglects some of the conditions of the actual experiment. The results of the comparisons indicate that effects of nonlinear propagation are readily observable between 100 and 375 m, despite overall sound pressure levels (OASPL) at 100 m that are less than 115 dB *re* 20  $\mu$ Pa for all measurements (see the legend in Fig. 5, where the maximum OASPL is 114.6 dB *re* 20  $\mu$ Pa). Based on OASPL alone, these results indicate that nonlinearity is very likely to occur in high-amplitude jet noise propagation, for which levels at 100 m may be 10–15 dB greater than for the MOAS. This corroborates earlier statements of Webster and Blackstock,<sup>2</sup> who reached a similar conclusion based on the results of their relatively short-range propagation experiments. Other comparisons shown in the present work are also important, specifically for the cases of propagation over greater distances and measurements made later in the afternoon, where agreement between the nonlinear model and experiment are not as good. They point to the need for the application of more sophisticated modeling techniques and additional research to better understand and predict the finite-amplitude propagation of continuous waveforms through a spatially and temporally variable atmosphere.

## ACKNOWLEDGMENTS

This work was supported by the Strategic Environmental Research and Development Program. The authors are grateful to Dr. Sally Anne McInerny at the University of Alabama for useful discussions and to the U.S. Army Research Labo-

ratory for their use of the Blossom Point test facility and the Mobile Acoustic Source. Additionally, the authors thank two anonymous reviewers for their helpful comments.

- <sup>1</sup>M. A. Theobald, “Experimental study of outdoor propagation of spherically spreading periodic acoustic waves of finite amplitude,” Technical Report ARL-TR-77-5, Applied Research Laboratories, The University of Texas at Austin, ADA 039020, 1977.
- <sup>2</sup>D. A. Webster and D. T. Blackstock, “Experimental investigation of outdoor propagation of finite-amplitude noise,” NASA Contractor Report 2992, Applied Research Laboratories, The University of Texas at Austin, 1978.
- <sup>3</sup>The MOAS has often been referred to as the “Mother Of All Speakers” (e.g., see Ref. 7).
- <sup>4</sup>V. W. Sparrow, K. L. Gee, J. M. Downing, and K. J. Plotkin, “Military aircraft noise and nonlinear acoustics,” *J. Acoust. Soc. Am.* **112**, 2214 (2002).
- <sup>5</sup>K. L. Gee, “Prediction of nonlinear jet noise propagation,” Ph.D. thesis, Graduate Program in Acoustics, The Pennsylvania State University, 2005.
- <sup>6</sup>F. M. Pestorius and D. T. Blackstock, “Propagation of finite-amplitude noise,” in *Finite-Amplitude Wave Effects in Fluids*, edited by L. Bjorno (IPC Science and Technology Press, Guildford, Surrey, England, 1973), pp. 24–29.
- <sup>7</sup>J. M. Sabatier, “Acoustical characterization of the mother of all speakers,” National Center for Physical Acoustics, The University of Mississippi, NCPA Control No.-JMS0593-1, May 1993.
- <sup>8</sup>K. Attenborough, S. I. Hayek, and J. M. Lawther, “Propagation of sound above a porous half-space,” *J. Acoust. Soc. Am.* **68**, 1493–1501 (1980).
- <sup>9</sup>G. A. Daigle, “Effects of atmospheric turbulence on the interference of sound waves above a finite impedance boundary,” *J. Acoust. Soc. Am.* **65**, 45–49 (1979).
- <sup>10</sup>R. V. Khokhlov, K. A. Naugol’nykh, and S. I. Soluyan, “Waves of moderate amplitudes in absorbing media,” *Acustica* **14**, 241–247 (1964).
- <sup>11</sup>D. T. Blackstock, “Generalized Burgers equation for plane waves,” *J. Acoust. Soc. Am.* **77**, 2050–2053 (1985).
- <sup>12</sup>R. O. Cleveland, J. P. Chambers, H. E. Bass, R. Raspet, D. T. Blackstock, and M. F. Hamilton, “Comparison of computer codes for the propagation of sonic boom waveforms through isothermal atmospheres,” *J. Acoust. Soc. Am.* **100**, 3017–3027 (1996).
- <sup>13</sup>A. D. Pierce, “Progressive wave equations and algorithms for sonic boom propagation,” *Proc. Noise-Con 93*, Noise Control Foundation, Poughkeepsie, New York, 1993, pp. 157–162.
- <sup>14</sup>M. O. Anderson, “The propagation of a spherical N wave in an absorbing medium and its diffraction by a circular aperture,” Technical Report ARL-TR-74-25, Applied Research Laboratories, The University of Texas at Austin, AD 787878, 1974.
- <sup>15</sup>H. E. Bass and R. Raspet, “Vibrational relaxation effects on the atmospheric attenuation and rise times of explosion waves,” *J. Acoust. Soc. Am.* **64**, 1208–1210 (1978).
- <sup>16</sup>L. B. Orenstein, “The rise time of N waves produced by sparks,” Technical Report ARL-TR-82-51, Applied Research Laboratories, The University of Texas at Austin, ADA 120817, 1982.
- <sup>17</sup>H. E. Bass, J. Ezell, and R. Raspet, “Effect of vibrational relaxation on rise times of shock waves in the atmosphere,” *J. Acoust. Soc. Am.* **74**, 1514–1517 (1983).
- <sup>18</sup>P. Blanc-Benon, B. Lipkens, L. Dallois, M. F. Hamilton, and D. T. Blackstock, “Propagation of finite amplitude sound through turbulence: Modeling with geometrical acoustics and the parabolic approximation,” *J. Acoust. Soc. Am.* **111**, 487–498 (2002).